PERGAMON

International Journal of Solids and Structures 37 (2000) 1549–1560

INTERNATIONAL JOURNAL OF SOLIDS and STRUCTURES

www.elsevier.com/locate/ijsolstr

3D multi-region BEM with corners and edges

X.-W. Gao*, T.G. Davies

Department of Civil Engineering, Glasgow University, Glasgow G12 8LT, UK

Received 3 October 1997; in revised form 8 September 1998

Abstract

A novel set of auxiliary equations, which supplement the fundamental boundary integral equations, for the treatment of corners and edges arising in discontinuous traction problems and at zonal intersections is derived. Based on these equations, an efficient linear 3D multi-region BEM algorithm is presented which can deal with arbitrarily many regions. Numerical examples demonstrate the effectiveness of this algorithm. © 1999 Elsevier Science Ltd. All rights reserved.

1. Introduction

In multi-region BEM algorithms in solid mechanics, the treatment of corners and edges requires particular attention since displacements are uniquely defined but the tractions are multi-valued. Development of such algorithms has important applications to cracked bodies, in the context of fracture mechanics (Raveendra and Cruse, 1989). One obvious way to tackle this problem is to 'round-off' corners and edges (Jaswon and Symm, 1977), but evidently this is not possible in multi-region problems. Alternatively, one could adopt the 'unique traction' assumption, namely that the tractions are equal on each contiguous surface (Cruse, 1974), although this violates the equilibrium condition. Although Lachat and Watson (1976) suggested that the errors incurred by this treatment are mainly confined to the corners, Alarcon et al. (1979) pointed out that this can lead to significant errors in the evaluation of the solution at interior points. In this paper, we also demonstrate that the 'unique traction' assumption yields unacceptable results at corners formed by the intersection of more than two regions. Avoiding the problem by using 'discontinuous elements', has significant disadvantages in terms of solution stability, computational effort and accuracy (Wilde, 1998).

To treat corners and edges rationally, it is necessary to introduce additional nodes and then develop auxiliary equations to determine the additional unknowns. For example, in the context of potential

* Corresponding author. Fax: +44-141-330-4557.
E-mail address: gao@civil.gla.ac.uk (X.-W. Gao)

PII: S0020-7683(98)00276-5

problems, Banerjee (1994) introduced a resistance relationship for this purpose. For 2D linear elasticity, Chaudonneret (1978) derived auxiliary relationships, based on the symmetry of the stress tensor and the invariance of the trace of the strain tensor. Wardle and Crotty (1978) and Mustoe (1980) used a polynomial interpolation to establish a relationship between tractions and displacements. Rudolphi (1983) described an implementation using quadratic elements for zoned problems, including discontinuous stress components. Zhang and Mukherjee (1991) generated auxiliary equations, for plane strain, by expressing the stresses at a corner as a linear combination of tractions and tangential displacement derivatives. Since all of these auxiliary equations are based on Hooke's law, they are restricted to linear analyses. Further, some workers assume an unique stress state (at corners), which is invalid in general (Zhang and Mukherjee, 1991). Moreover, methods proposed for 2D applications are generally insufficient in 3D.

In this paper, a novel set of auxiliary equations is derived from the symmetry property and the equilibrium equations of the stress tensor. These equations do not depend on the displacement field, nor on Hooke's law, which suggests wider applications to non-linear and dynamic problems. Further, we treat the multi-region problem for more than two intersecting zones for the first time.

2. Problems of corners and edges

In elasticity problems, the BEM algorithm can be derived by discretizing the boundary of the problem into elements as follows:

$$cu + \sum_{e=1}^{M_e} u^e \left(\int_{\Delta S_e} T^e N^e \, \mathrm{d}S \right) = \sum_{e=1}^{M_e} t^e \left(\int_{\Delta S_e} U^e N^e \, \mathrm{d}S \right) \tag{1}$$

where c is constant associated with the geometry, M_e is the total number of elements, u^e and t^e are the nodal displacements and tractions over the e-th element, N^e are the interpolation functions, and U^e and T^e are the Kelvin's fundamental solutions for displacements and tractions, respectively.

At zonal intersections, the displacements are uniquely defined but the tractions are multi-valued since each surface has, in general, different outward normals. We define additional (coincident) nodes at the intersection so that each node is shared by not more than two regions. Thus, for N original boundary nodes (including corner nodes) and $\tilde{N}$ additional nodes, the resulting system equations are:

$$[H]\{u\} = [G]\{t\} \tag{2}$$

where, $[H]$ is a $3N \times 3N$ matrix and $[G]$ is a $3N \times 3(N + \tilde{N})$ matrix for 3D problems. Since the system equations provide only $3N$ equations, $3\tilde{N}$ additional (auxiliary) equations must be established.

3. Auxiliary equations for corners and edges

The tractions can be expressed in terms of stresses as:

$$t_i = \sigma_{ij} n_j \tag{3}$$

in which, n_j are the components of the unit outward normal n and the repeated index represents summation. For a point on a surface, we introduce a local Cartesian co-ordinate system x_i', $i = 1$–3, with the axes x_1' and x_2' tangential to the surface and x_3' in the n-direction (Fig. 1).

The global quantities, co-ordinates and tractions, can be transformed into the local co-ordinate system:

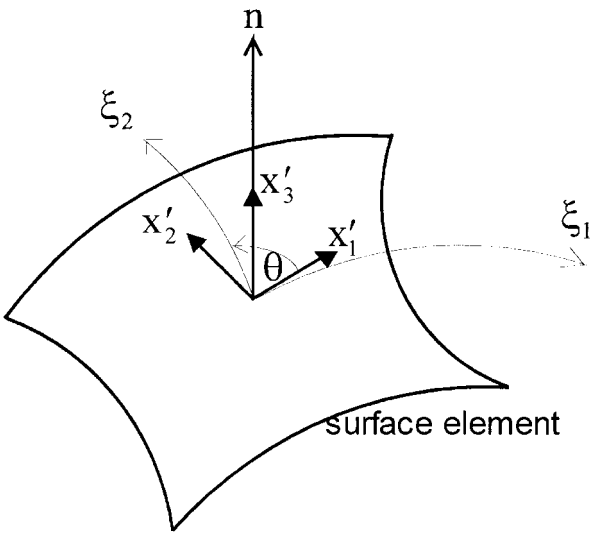

Fig. 1. Three-dimensional local orthogonal set of axes.

$$x_i' = L_{ij}x_j \tag{4}$$

$$t_i' = L_{ij}t_j \tag{5}$$

where

$$L_{ij} = \frac{\partial x_i'}{\partial x_j}. \tag{6}$$

This leads to the relationships:

$$\frac{\partial t_k'}{\partial x_k'} = L_{ki}\frac{\partial \sigma_{ij}}{\partial x_k'}n_j = \frac{\partial \sigma_{ij}}{\partial x_i}n_j. \tag{7}$$

Using the equilibrium equation, namely:

$$\frac{\partial \sigma_{ij}}{\partial x_i} = \rho \ddot{u}_j - f_j \tag{8}$$

we obtain:

$$\frac{\partial t_k'}{\partial x_k'} = (\rho \ddot{u}_i - f_i)n_i \tag{9}$$

in which, f_i and $\ddot{u}_i$ are the components of the body force and acceleration vectors, respectively, and ρ is the mass density.

This (auxiliary) equation is a general relationship between the tangential components ($k = 1$–2 only) of the traction vector and is valid whether the stress field is continuous or discontinuous. Although derived for 3D problems, it is also valid for 2D problems (with $k = 1$ only). After some manipulations (see Appendix) we obtain, excluding body forces for simplicity:

$$\frac{\partial \xi_k}{\partial x'_p} L_{pi} \frac{\partial N_\alpha}{\partial \xi_k} t_i^\alpha = 0 \tag{10}$$

where t_i^α is the i-th component of the traction at the α-th node.

Now eqn (10) can be readily implemented within the BEM code. Although this equation provides sufficient equations in 2D, it may be insufficient in some 3D problems. In such cases, we derive supplementary equations by invoking the assumption that the stress tensor is continuous at a corner (edge). For a corner, at the intersection of surfaces S_a and S_b, (with unit outward normals n^a and n^b, respectively) we have:

$$n_i^b t_i^a = n_i^b \sigma_{ij} n_j^a$$

$$n_i^a t_i^b = n_i^a \sigma_{ij} n_j^b. \tag{11}$$

From the symmetry of the stress tensor, it follows that:

$$n_i^b t_i^a = n_i^a t_i^b. \tag{12}$$

The 2D form of this equation was first obtained by Chaudonneret (1978). For single region problems, eqn (10) yields one equation for each node defined at a corner (edge) while eqn (12) produces one equation for two nodes with different normals. However, at an interface node shared by two zones, these equations can be applied to one zone only.

For the 3D two-zone edge intersection (with two nodes), and after consideration of the interface conditions, there remains nine unknowns (three displacement components and six traction components). Six equations are provided by the BEM and two auxiliary equations can be obtained from eqn (10) and one from eqn (12). For the 3D three-zone edge intersection (with three nodes), there are twelve unknowns. While the BEM formulation provides only nine equations, six auxiliary equations (three from eqn (10) and another three from eqn (12)) are available. As expected, eqn (10) provides better results, since this avoids the restrictive 'continuous stress' assumption. In general, the number of auxiliary equations which must be invoked for corner or edge points is

$$m = d^*(n - p + 1) \tag{13}$$

where, $d = 2(3)$ for 2D (3D) problems, n is the number of the nodes associated with the point, and p is the number of the zones meeting at that point.

4. Multi-region BEM algorithm

Various assembly methods can be used to establish the multi-region system equations (Banerjee and Butterfield, 1981; Brebbia et al., 1984; Kane et al., 1990). In the present study, we employ a different substructure technique. The discretized BEM eqn (2) for the i-th zone can be expressed as:

$$[H^i]\{u^i\} = [G^i]\{t^i\} \tag{14}$$

$[H^i]$ and $[G^i]$ are square and rectangular coefficient matrices, respectively, and $\{u^i\}$ and $\{t^i\}$ are column vectors of nodal displacements and tractions.

We collect the nodes for each zone into two sets. The first set includes the nodes solely associated with a single region. This set of nodes are called 'external nodes' and will be eliminated at the zonal

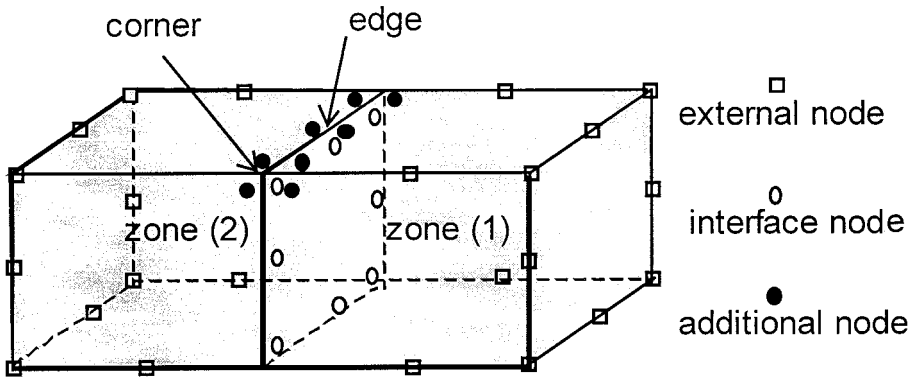

Fig. 2. A two-zone problem.

level. The remaining nodes reside on region-to-region interfaces. For convenience, all the nodes associated with the corner and edge points are classified into the latter set. Eqn (14) can then be written in the form:

$$\begin{bmatrix} [H^i_{EE}] & [H^i_{EI}] \\ [H^i_{IE}] & [H^i_{II}] \end{bmatrix} \begin{Bmatrix} \{u^i_E\} \\ \{u^i_I\} \end{Bmatrix} = \begin{bmatrix} [G^i_{EE}] & [G^i_{ES}] \\ [G^i_{IE}] & [G^i_{IS}] \end{bmatrix} \begin{Bmatrix} \{t^i_E\} \\ \{t^i_S\} \end{Bmatrix} \tag{15}$$

in which, the subscript I denotes displacements at the region-to-region interface nodes (Fig. 2); the subscript S denotes tractions at the system nodes (interface and additional nodes), and the subscript E denotes the quantities at the remaining external nodes associated with a single region. The boundary conditions are applied at the zonal level and, after shifting the unknowns to the left-hand side, the block-banded matrix, eqn (15) becomes, after some manipulation:

$$[C^i_{II}]\{u^i_I\} = [D^i_{IS}]\{t^i_S\} + \{Y^i_I\}. \tag{16}$$

It is convenient to define a global traction vector $\{t_S\}$ for all the interface nodes and all the additional nodes, such that the local traction vector $\{t^i_S\}$ can be expressed in terms of $\{t_S\}$ by the equation:

$$\{t^i_S\} = [L^{ti}]\{t_S\} \tag{17}$$

where $[L^{ti}]$ is the 'traction location matrix' for zone i, consisting only of 0, 1 and −1. The construction of $[L^{ti}]$ takes into account the interface equilibrium conditions; for example, the condition $\{t^1_S\} = -\{t^2_S\}$ on the interface shared by zone 1 and zone 2.

We also define a global displacement vector $[u_I]$ for all the interface and additional nodes and introduce a displacement location matrix $[L^{ui}]$ for zone i, consisting of 0, 1, thus:

$$\{u^i_I\} = [L^{ui}]\{u_I\} \tag{18}$$

where $[L^{ui}]$ identifies the zonal compatibility conditions.

Assembling the zonal equations, together with the auxiliary equations yields the final system equations:

$$\begin{bmatrix} -[D_{IS}^{1}][L^{t1}] & [C_{II}^{1}][L^{u1}] \\ -[D_{IS}^{2}][L^{t2}] & [C_{II}^{2}][L^{u2}] \\ \cdots & \cdots \\ -[D_{IS}^{m}][L^{tm}] & [C_{II}^{m}][L^{um}] \\ [E\ ] & [0] \end{bmatrix} \begin{Bmatrix} \{t_S\} \\ \{u_I\} \end{Bmatrix} = \begin{Bmatrix} \{Y_I^1\} \\ \{Y_I^2\} \\ \cdots \\ \{Y_I^m\} \\ \{Y_A\} \end{Bmatrix} \tag{19}$$

in which, $[E_A]$ and $\{Y_A\}$ are generated from the auxiliary equations and the traction boundary conditions. This assembly technique permits simultaneous solution of both displacements and tractions for the interface and additional nodes.

If a region is not explicitly prevented from undergoing rigid body displacements, then the solution technique fails. In this situation, the SVD technique (Press et al., 1992) provides a convenient means of overcoming the problem, albeit at the expense of greater computational time. Numerical problems may also occur if the ratio of the values of the coefficient matrices of $\{t_S\}$ and $\{u_I\}$ become unduly large. This difficulty can be circumvented by normalising the coefficients by a representative value of shear modulus. Evidently, the same representative value must be used for all zones.

5. Numerical examples

The 3D elastostatic multi-region BEM computer code (ESMI-3D), written in FORTRAN 77, can deal with arbitrarily many zones using 4-node linear and 8-node quadratic elements. An infinite boundary element technique (Davies and Bu, 1996; Gao and Davies, 1998) provides an efficient means to deal with semi-infinite domains. Two representative examples, solved using single precision arithmetic, are

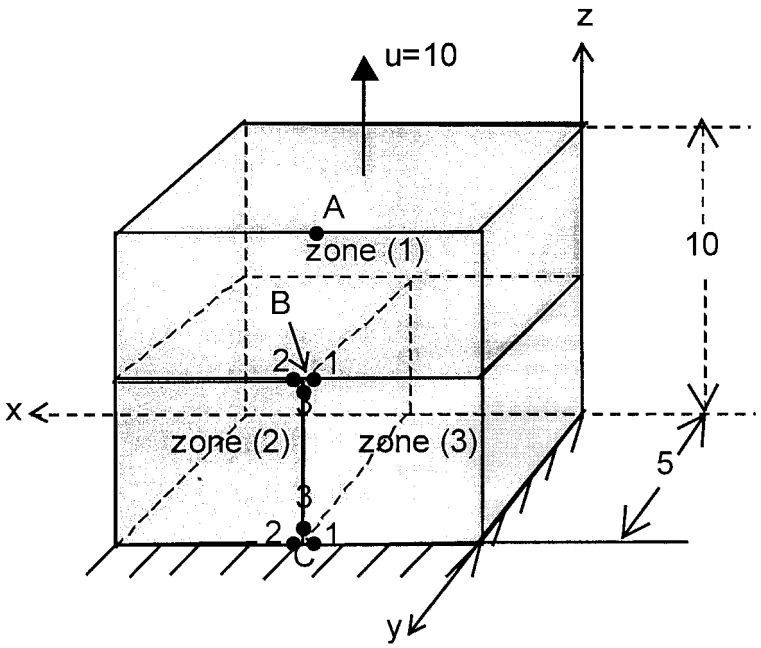

Fig. 3. A cube undergoing a displacement $u = 10$.

Table 1
Calculated tractions t_z for interface nodes

Point	Node	Analytical solution	Auxiliary equation	Unique at C	Unique at B
A		1.0	1.0000	0.9995	0.4857
B	1	−1.0	−1.0000	−1.0089	
	2	−1.0	−1.0000	−0.9994	−7.6385
	3	0.0	0.0000	0.0030	
C	1	−1.0	−1.0000		−24.0765
	2	−1.0	−1.0000	−0.0021	24.1647
	3	0.0	0.0000		−27.6547

($E_1 = E_2 = E_3 = 1$ and $v_1 = v_2 = v_3 = 0$).

Table 2
Calculated displacements at point B

	Analytical solution	Auxiliary equation	Unique at C	Unique at B
u_x	0.0	0.0000	−0.0005	−3.7981
u_y	0.0	0.0000	−0.0006	−1.7823
u_z	5.0	5.0000	4.9929	−0.8397

($E_1 = E_2 = E_3 = 1$ and $v_1 = v_2 = v_3 = 0$).

presented here for illustrative purposes. For any interface node, the tractions are referred to the surface of the lower numbered zone.

5.1. Example 1: three-zoned cube

The first example is a cube, consisting of three zones, subjected to uniform extension, i.e. $u = 10$ (Fig. 3). Both the central point B and the bottom central point C are represented by three independent nodes, one for each face. The cube is discretised into 88 eight-noded elements (40, 24 and 24 for zones 1, 2 and 3, respectively) with 212 original nodes and 20 additional nodes. All the elements have the same dimension (2.5×2.5).

To begin with, we assume that the mechanical properties of the three zones are the same. Table 1 shows the computed tractions t_z for the nodes associated with points A, B and C. Table 2 shows the displacements at the point B, where the column headed by the title 'Auxiliary equation' indicates the results computed using the auxiliary equations presented in this paper, and the columns headed by the titles 'Unique at C' and 'Unique at B' denote the results obtained by defining only one node at points C and B, respectively. It is evident that these simplified methods fail to capture the correct solution.

Inspection of these tables shows that the auxiliary equation algorithm presented in this paper gives results in excellent agreement with the analytical solutions. The unique (single) node method can only provide approximate results for two-zone intersections, while for three-zone intersections, the computed results are unacceptable.

We now consider a case where the mechanical properties of each zone are different. The tractions at points B and C computed using the present algorithm are given in Table 3. The unique node method was also applied to this case, with similar conclusions to the above.

Table 3
Traction values

Point	Node	t_x	t_y	t_z
B	1	1.5749	3.3347	−0.6671
	2	0.8857	−2.4120	−6.1122
	3	−0.8602	−3.2954	1.1881
C	1	−2.4271	−5.6103	−0.4534
	2	−0.4655	3.2384	−6.6272
	3	−1.9077	−5.1288	2.1881

($E_1 = 5$, $E_2 = 3$, $E_3 = 1$, and $v_1 = v_2 = v_3 = 0.2$).

Table 4
Radial displacements by different methods

Point	Analytical solution	Auxiliary equation	Unique at D	Unique at B
A	15.275	15.124	14.691	14.540
B	8.613	8.587	8.107	7.731
C	6.825	6.796	6.334	5.928

($E_1 = E_2 = E_3 = E_4 = 1$).

5.2. Example 2: four-zoned thick cylinder

The second (3D) example is a thick circular cylinder subjected to internal pressure, $p = 1$. Figure 4 shows the mesh employed which was composed of four zones with 48 eight-noded elements (12 elements for each zone), with 131 original nodes and 63 additional nodes. A quarter of the cylinder is analysed.

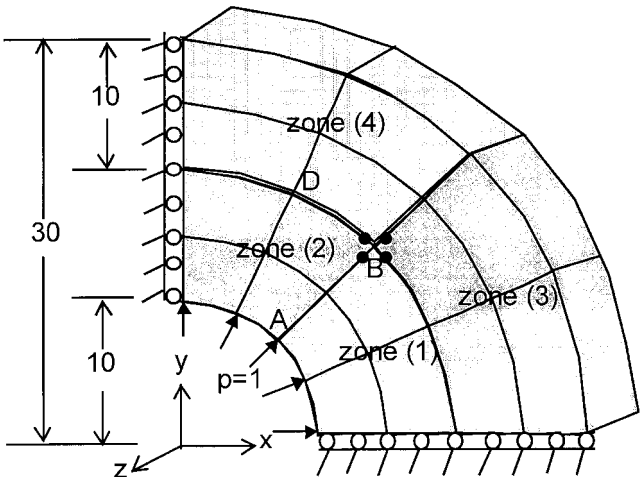

Fig. 4. Cylinder subjected to internal pressure.

The x–y plane (at $z = 20$) is subjected to 'roller' boundary conditions ($u_z = 0$) and symmetry is assumed about the $z = 0$ plane to simulate a state of plane strain. The vertical ($x = 0$) and horizontal ($y = 0$) boundaries are also 'roller' supports (i.e. $u_x = 0$ and $u_y = 0$, respectively).

As before, we first consider the case of identical mechanical properties in all four regions ($E = 1$, $v = 0.3$). Figs. 5 and 6 show the variations of the radial displacements and circumferential stresses along the radial (r) direction. We observe that the auxiliary equation algorithm gives excellent agreement with the analytical solutions. The small discrepancies at the inner and outer surfaces may be due to the rather coarse mesh adopted.

To compare the results obtained by analytical, auxiliary, and unique node methods, Table 4 shows the

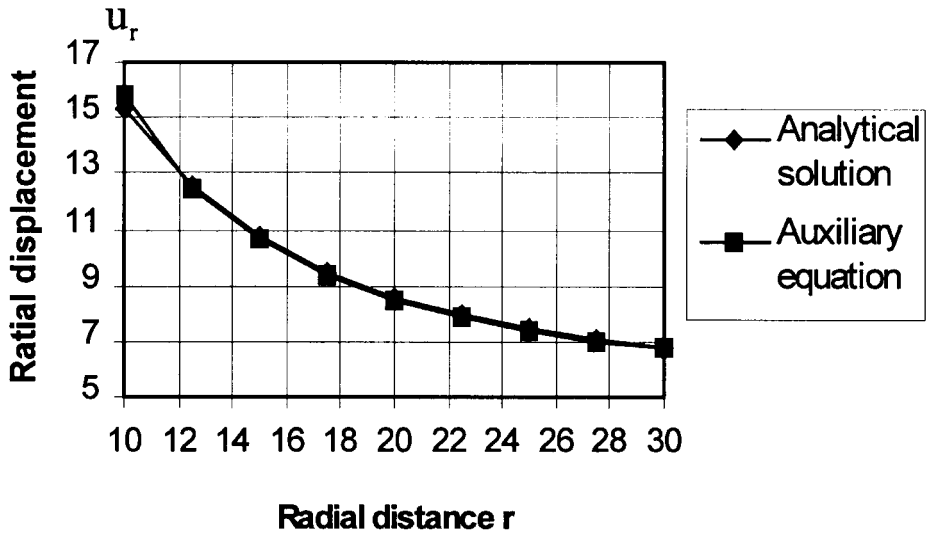

Fig. 5. Variation of radial displacement vs radial distance ($E_1 = E_2 = E_3 = E_4 = 1$).

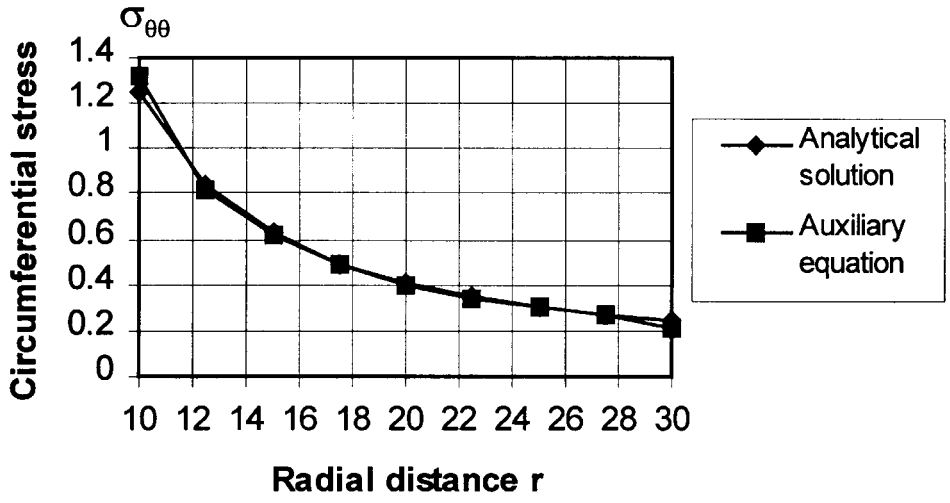

Fig. 6. Variation of circumferential stress vs radial distance ($E_1 = E_2 = E_3 = E_4 = 1$).

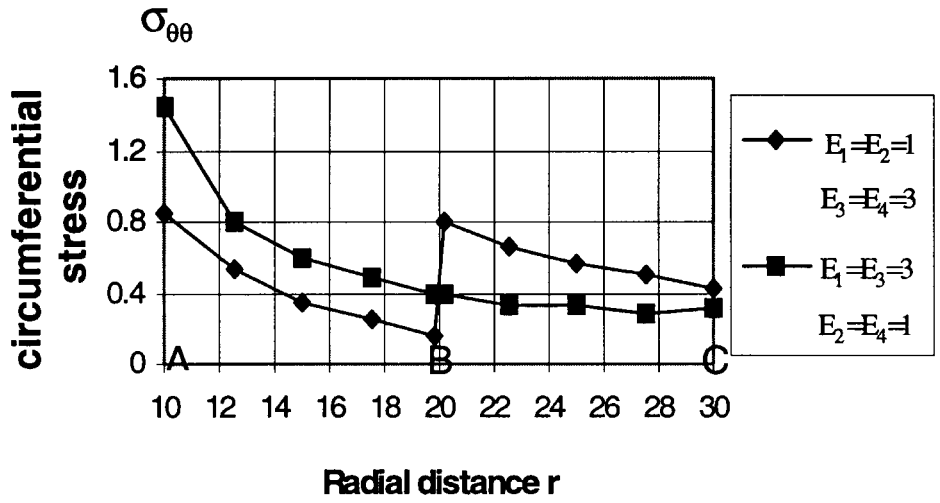

Fig. 7. Variation of circumferential stress along line ABC.

radial displacements at different points. Again, it is evident that a 'simple' approach is inadequate. To examine the effect of zonal inhomogeneity on the circumferential stress along the radius ABC (in Fig. 4), analyses have been carried out for the two cases: ($E_1 = E_2 = 1, E_3 = E_4 = 3$) and ($E_1 = E_3 = 3, E_2 = E_4 = 1$). In these analyses, the Poisson's ratio is taken to be 0.3 in all regions. Fig. 7 shows the results for the two cases. The radial displacement along the radius ABC is plotted in Fig. 8 From Fig. 7, we observe that the circumferential stress is discontinuous at the point B (more starkly for the first case) because of the non-homogeneous material properties at this interface. This phenomenon cannot be captured using the conventional multi-region BEM program.

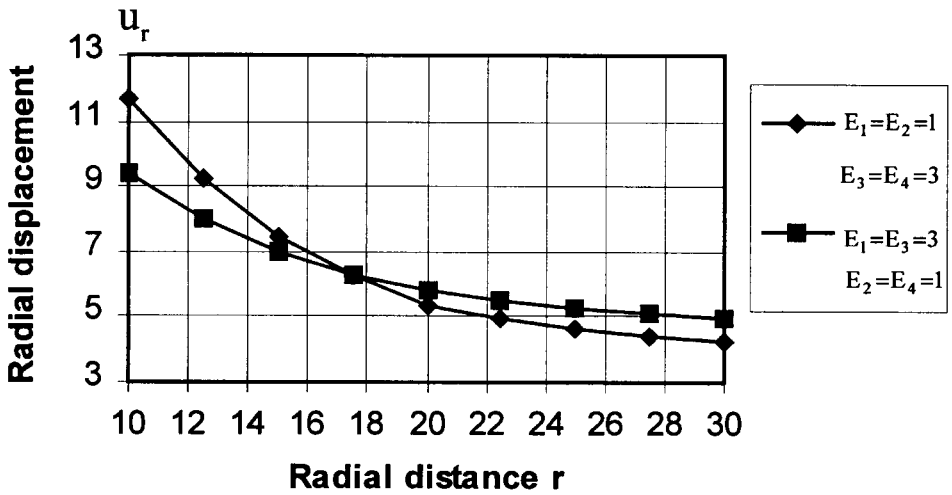

Fig. 8. Variation of radial displacement along line ABC.

6. Conclusions

A novel method has been derived to establish the auxiliary equations necessary to deal with the corner problem in 3D multi-region mechanics. A significant feature of the method is that it does not depend on Hooke's law. A strategy for solving the resulting system of equations is outlined. Some illustrative numerical results are given which demonstrate the validity of the algorithm, and also the shortcomings of algorithms which neglect the rigorous treatment of the corner problem.

Acknowledgements

This project was supported by grants from the National Natural Science Fund of P.R. China (No. 19362003) and the Faculty of Engineering, University of Glasgow, U.K.

Appendix

Referring to Fig. 1, the components of the co-ordinate system can be expressed in terms of the orthogonal axes system as follows (Lachat, 1975):

$$\frac{\partial \xi_1}{\partial x_1'} = \frac{1}{|m_1|}; \quad \frac{\partial \xi_1}{\partial x_2'} = \frac{-\cos\theta}{|m_1|\sin\theta};$$

$$\frac{\partial \xi_2}{\partial x_1'} = 0; \quad \frac{\partial \xi_2}{\partial x_2'} = \frac{1}{|m_2|\sin\theta} \tag{A1}$$

where

$$|m_k| = \sqrt{\left(\frac{\partial x_1}{\partial \xi_k}\right)^2 + \left(\frac{\partial x_2}{\partial \xi_k}\right)^2 + \left(\frac{\partial x_3}{\partial \xi_k}\right)^2} \tag{A2}$$

$$\cos\theta = \frac{1}{|m_1||m_2|}\frac{\partial x_i}{\partial \xi_1}\frac{\partial x_i}{\partial \xi_2} \tag{A3}$$

$$x_i = N_\alpha(\xi_1, \xi_2)x_i^\alpha \tag{A4}$$

in which, $k = 1, 2$; $i = 1, 2, 3$ and $N_\alpha(\xi_1, \xi_2)$ are the shape functions and x_i^α is the i-th component of the coordinates with respect to α-th node, with α taking the values through 1 to the number of element nodes. From eqn (5):

$$\frac{\partial t_k'}{\partial x_k'} = L_{pi}\frac{\partial t_i}{\partial \xi_k}\frac{\partial \xi_k}{\partial x_p'} \tag{A5}$$

in which, L_{pi} ($p = 1, 2$) are the direction cosines of the local axes, x_1' and x_2', respectively, i.e.

$$L_{1i} = \frac{1}{|m_1|}\frac{\partial x_i}{\partial \xi_1}, \quad i = 1, 2, 3 \tag{A6}$$

$$L_{21} = n_2 L_{13} - n_3 L_{12}$$

$$L_{22} = n_3 L_{11} - n_1 L_{13}$$

$$L_{23} = n_1 L_{12} - n_2 L_{11}. \tag{A7}$$

Substituting eqn (A5) into eqn (9) and noticing that $t_i = N_\alpha t_i^\alpha$, it follows that:

$$\frac{\partial \xi_k}{\partial x'_p} L_{pi} \frac{\partial N_\alpha}{\partial \xi_k} t_i^\alpha = (\rho \ddot{u}_i - f_i) n_i \tag{A8}$$

where t_i^α is the i-th component of the traction at the α-th node.

References

Alarcon, A., Martin, A., Paris, F., 1979. Boundary elements in potential and elasticity theory. Comput. Struct. 10, 351–362.

Banerjee, P.K., 1994. The Boundary Element Methods in Engineering. McGraw–Hill Book Company, pp. 73–75.

Banerjee, P.K., Butterfield, R., 1981. Boundary Element Methods in Engineering Science. McGraw–Hill Book Company (U.K.) Ltd, pp. 168–176.

Brebbia, C.A., Telles, J.C.F., Wrobel, L.C., 1984. Boundary Element Techniques. Springer–Verlag, Berlin and New York.

Chaudonneret, M., 1978. On the discontinuity of the stress vector in the boundary integral equation method for elastic analysis. In: Brebbia, C.A. (Ed.), Recent Advances in Boundary Element Methods. Pentech Press, London.

Cruse, T.A., 1974. An improved boundary-integral equation method for three dimensional elastic stress analysis. Comput. Struct. 4, 741–754.

Davies, T.G., Bu, S., 1996. Infinite boundary elements for the analysis of halfspace problems. Comput. Geotech. 19, 137–151.

Gao, X.W., Davies, T.G., 1998. 3D infinite boundary elements for halfspace problems. Engng Anal. Bound. Elem. 21, 207–213.

Jaswon, M.A., Symm, G.T., 1977. Integral Equation Methods in Potential Theory and Elastostatics. Academic Press, London.

Kane, J.H., Kumar, B.L.K., Saigal, S., 1990. An arbitrary multi-zone condensation technique for boundary element design sensitivity analysis. AIAA J. 28, 1277–1284.

Lachat, J.C., 1975. A Further Development of the Boundary Integral Technique for Elastostatics. Ph.D. thesis, University of Southampton.

Lachat, J.C., Watson, J.O., 1976. Effective numerical treatment of boundary integral equation. Int. J. Num. Meth. Engng 10, 991–1005.

Mustoe, G.G.W., 1980. A Combination of the Finite Element Method and Boundary Integral Procedure for Continuum Problems. Ph.D. thesis, University of Wales, University College, Swansea.

Press, W.H., Teukolsky, S.A., Vetterling, W.T., Flannery, B.P., 1992. Numerical Recipes in FORTRAN: The Art of Scientific Computing, 2nd ed., Cambridge University Press.

Raveendra, S.T., Cruse, T.A., 1989. BEM analysis of problems of fracture mechanics. In: Banerjee, P.K., Wilson, R.B. (Eds.), Industrial Applications of Boundary Element Methods. Elsevier Applied Science, London and New York, pp. 187–204.

Rudolphi, T.J., 1983. An implementation of the boundary element method for zoned media with stress discontinuities. Int. J. Num. Meth. Engng 19, 1–15.

Wardle, L.J., Crotty, J.M., 1976. Two-dimensional boundary integral equation analysis for non-homogeneous mining applications. In: Brebbia, C.A. (Ed.), Recent Advances in Boundary Element Methods. Pentech Press, London, pp. 233–249.

Wilde, A.J., 1998. A Hypersingular Dual Boundary Element Formulation for Three-dimensional Fracture Analysis. Ph.D. thesis, Wessex Institute of Technology, University of Wales, pp. 67.

Zhang, Q., Mukherjee, S., 1991. Design sensitivity coefficients for linear elastic bodies with zones and corners by the derivative boundary element method. Int. J. Solids Struct. 27, 983–998.